Mechanics of cell spreading within 3D-micropatterned environments†‡

Marion Ghibaudo,[a] Jean-Marc Di Meglio,[a] Pascal Hersen[ab] and Benoit Ladoux*[ab]

Received 21st July 2010, Accepted 2nd November 2010
DOI: 10.1039/c0lc00221f

Most tissue cells evolve *in vivo* in a three-dimensional (3D) microenvironment including complex topographical patterns. Cells exert contractile forces to adhere and migrate through the extracellular matrix (ECM). Although cell mechanics has been extensively studied on 2D surfaces, there are too few approaches that give access to the traction forces that are exerted in 3D environments. Here, we describe an approach to measure dynamically the contractile forces exerted by fibroblasts while they spread within arrays of large flexible micropillars coated with ECM proteins. Contrary to very dense arrays of microposts, the density of the micropillars has been chosen to promote cell adhesion in between the pillars. Cells progressively impale onto the micropatterned substrate. They first adhere on the top of the pillars without applying any detectable forces. Then, they spread along the pillar sides, spanning between the elastic micropillars and applying large forces on the substrate. Interestingly, the architecture of the actin cytoskeleton and the adhesion complexes vary over time as cells pull on the pillars. In particular, we observed less stress fibers than for cells spread on flat surfaces. However, prominent actin stress fibers are observed at cell edges surrounding the micropillars. They generate increasing contractile forces during cell spreading. Cells treated with blebbistatin, a myosin II inhibitor, relax their internal tension, as observed by the release of pillar deformations. Moreover, cell spreading on pillars coated with ECM proteins only on their tops are not able to generate significant traction forces. Taken together, these findings highlight the dynamic relationship between cellular forces and acto-myosin contractility in 3D environments, the influence of cytoskeletal network mechanics on cell shape, as well as the importance of cell–ECM contact area in the generation of traction forces.

Introduction

Cell adhesion plays a central role in many biological processes such as tumor formation, tissue development and homeostasis, including the responses to wounds and inflammation. In routine 2D cell culture, the processes of cell spreading, adhesion and migration have been studied in detail.[1] To adhere and migrate, tissue cells exert contractile forces on their substrate.[2] Such forces are generated by the cell's own contractile apparatus. The primary sites of cell adhesion to the substrate are focal adhesions.[3] These complex multimolecular assemblies link the extracellular matrix (ECM), *via* membrane-bound receptors, to the cell's actin cytoskeleton.[4] Focal adhesions are therefore the sites at which forces are transmitted to the substrate through acto-myosin contraction. Consequently, as they pull on their surroundings, tissue cells reorganize their acto-myosin apparatus and their focal adhesion sites.[5]

Physical factors of the cellular microenvironment that are sensed by cells—such as topography, rigidity and forces—can modulate the cell tension and the traction forces exerted by cells and are thus crucial for understanding cell functions.[5–7] For instance, matrix stiffness and external forces can affect gene expression,[8] cell adhesion[9–11] and spreading,[12–14] as well as cell migration[15,16] in 2D cell culture. Furthermore, nano- and micro-patterned techniques on 2D surfaces have shown that the ECM topography is crucial for cell organization and adhesion.[17,18]

The natural ECM of cells is a complex 3D fibrous meshwork with a wide distribution of fibers and gaps that exhibit complex physical and geometrical cues.[19] Compared to cells on 2D surfaces, cells *in vivo* or embedded in 3D reconstituted matrices are subjected to 3D interactions that induce different morphology and behavior.[20] Previous studies have shown that cells could exert large forces as they spread between two surfaces with one of them soft enough to be deflected by the cells.[7,21] However, the role of substrate topography on cell shape, cytoskeleton organization and force generation is poorly understood for cells adhering in a 3D environment. The complexity of *in vivo* 3D environments makes it difficult to study the influence of external factors on these various parameters. Remodeling the 3D ECM can indeed affect simultaneously the physical and biochemical characteristics of the matrix.

In this context, microfabricated substrates appear as useful tools to study the influence of physical parameters on cell adhesion. Micropatterned substrates of ECM proteins led to important findings in the regulation of cell adhesion on confined geometries.[22,23] A recent study has evidenced that cells migrating on 1D micropatterned lines share many similarities with cell migration in 3D.[24] Micro-structured substrates made of grooves and pillars have been developed for mimicking 3D environments

[a]*Laboratoire Matière et Systèmes Complexes (MSC), Université Paris-Diderot & CNRS UMR 7057, Bâtiment Condorcet, Paris, France. E-mail: benoit.ladoux@univ-paris-diderot.fr; Fax: +33 (0)1 57 27 62 11; Tel: +33 (0)1 57 27 70 35*
[b]*Mechanobiology Institute (MBI), National University of Singapore (NUS), Singapore*

† Published as part of a LOC themed issue dedicated to French Research: Guest Editor Professor Jean-Louis Viovy.

‡ Electronic supplementary information (ESI) available: Fig. S1–S3; Movies S1–S3. See DOI: 10.1039/c0lc00221f/

and for studying cellular responses to topography.[25–30] Another example is the use of substrates composed of flexible micropillar arrays to quantify cellular traction forces on 2D surfaces[31–33] as well as forces generated by 3D microtissues[34] or myocytes.[30,35]

In this study, we present an approach to measure the forces of single cells while they spread into 3D flexible microstructured environments. We have adapted and combined previous experimental techniques[29,33] available in our lab, to have access to forces exerted by cells as they invade and span within an array of microfabricated elastic pillars. The micropillars are made from a silicone elastomer and deflect as cells spread along the pillars. The force generation mechanism is mostly due to prominent actin stress fibers that wrap around the pillars. This is confirmed by the inhibition of myosin II that induces a relaxation of the forces. Altogether our findings demonstrate that cell spreading is crucial for the force generation mechanism within 3D microstructures and traction forces within 3D environments induce a reorganization of acto-myosin contractility.

Materials and methods

Cell culture and pharmacological treatments

REF52 fibroblasts were maintained at 37 °C in a humidified atmosphere of 5% CO_2 and 95% air in Dulbecco's modified Eagle medium (DMEM) containing 10% bovine calf serum, 100 U mL^{-1} penicillin, 100 μg mL^{-1} streptomycin and 100 μg mL^{-1} glutamine. REF52 cells expressed a stable paxillin-YFP (kindly provided by A. Bershadsky). Blebbistatin was added to the medium at a 50 μM concentration. To avoid its phototoxic effect we filtered the incident light with a 03 FCG 089 filter (Melles Griot).

Cell staining

For fluorescence staining, cells were fixed with 4% paraformaldehyde in PBS for 30 min at room temperature, rinsed three times with PBS and permeabilized (50 mM of NH_4Cl in PBS for 10 min and 0.1% Triton X-100 in PBS for 4 min). For actin labeling, cells were then stained with either Oregon green-conjugated phalloidin at a dilution of 1 : 100 or Phalloidin-FluoProbes® 547H (Interchim, Montluçon, France) at a dilution of 1 : 40. For calcein staining, cells were loaded with 0.2 μM of Calcein AM (BD Biosciences) for 30 min before trypsinization. Nucleus staining was performed with DAPI.

Substrate microfabrication and mechanical properties

Polydimethylsiloxane (PDMS, Sylgard 184, Dow Corning) micropillar arrays were prepared according to du Roure *et al.*[33] PDMS mix was poured over a silicon wafer, cured at 65 °C for 15 ±2 h and peeled off the wafer in dry conditions. We used a consistent cure time of 15 ±2 h at 65 °C corresponding to a Young's modulus of 2 ±0.1 MPa. Scanning electron microscopy (SEM) allowed us to measure the dimensions of the pillars as previously described.[33]

The size and shape of the micropillars, their spacing or other geometrical parameters were varied. After peeling off the PDMS mold from the wafer, its surface displayed an hexagonal array of cylindrical pillars. We used a constant length (L) and diameter (d) of 20 μm and 5 μm, respectively. The spacing from edge to edge of the pillars (S) was varied from 4 μm to 12 μm (see Fig. 1) allowing cells to spread within the microstructures. Experiments were conducted on micropillar substrates of different surface densities from 10 to 33%. In the present study, the pillars were soft enough to be significantly deformed by cells only in the lateral direction. Indeed the spring constants of the pillars under compression, k_n, or shear, k_t, are given by the following formulas:

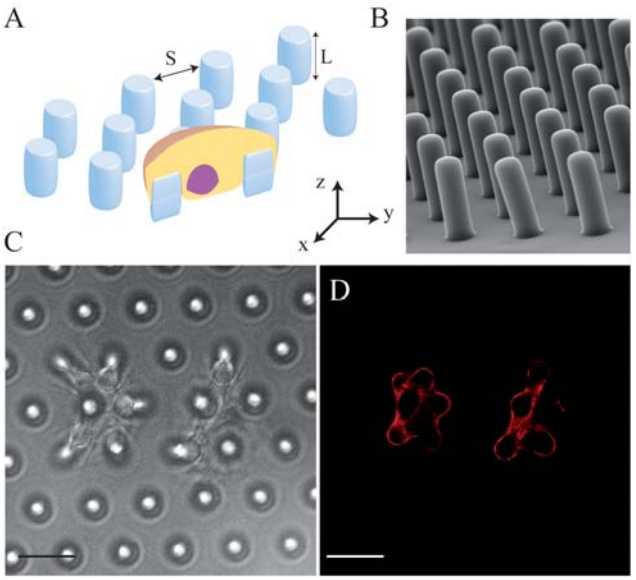

Fig. 1 (A) Schematic representation of our experimental set-up. (B) Scanning electron micrograph of the micropillar substrate (20 μm high). (C) Bright field image of the micropillar substrate deformed by the spreading of two individual cells (scale bar = 15 μm). (D) Cell shapes after they spread into micropillar substrates shown by the immunofluorescent staining of actin cytoskeleton. Cell fixation was performed 90 min after plating cells on the substrate (scale bar = 15 μm).

$$k_n \propto E \cdot \frac{d^2}{L} \quad \text{and} \quad k_t \propto E \cdot \frac{d^4}{L^3}$$

where E, L and d are the Young's modulus of the PDMS, the length and the diameter of the pillars, respectively. The pillar spring constants were $\simeq$1000 and 23 nN μm^{-1} for k_n and k_t, respectively.

Substrate biofunctionalization

PDMS micropillar substrates were coated with fibronectin. Only the top of the pillars was coated with fluorescently labeled fibronectin (Cy3, Amersham Biosciences, Orsay, France). In this case, we used a modified procedure of micro-contact printing.[36] Briefly, a stamp of flat PDMS was inked with a PBS solution containing 50 μg ml^{-1} of fibronectin and 5 μg ml^{-1} of Cy3 labeled fibronectin. The stamps were then dried under argon and placed against the μFSA (micro Force Sensor Array) for 15 min. Substrates were then either immersed with a solution of fibronectin (20 μg ml^{-1}) (Sigma-Aldrich) in PBS buffer for 2 h to allow cell spreading in between the pillars or silanized and incubated with 20 mg ml^{-1} reactive PEG (ShearWater mPEG-MAL MW, Nektar Therapeutics) in PBS for 1 h to prevent cell adhesion along the pillars.[16]

Time-lapse video microscopy and measurements

We acquired time-lapse images using an Olympus BX51 upright microscope (Olympus), equipped with an on-stage heater maintaining the temperature at 37 °C (LIS, Basel, Switzerland). To prevent gas exchange and water evaporation, the culture medium was covered with a thin layer of mineral oil after addition of 45 mM HEPES into the solution to keep a constant pH. Images were acquired through an Olympus 60× water objective (NA 0.90) by a HQ^2 camera (Roper Scientific) controlled by Metamorph software (Universal Imaging Corporation). Time-lapse sequences were acquired for up to 2 h using a 30 s time-step.

We used a home-made multi-particle tracking routine that allowed us to detect micropillar positions for each image of the stack.[33] We detected the fluorescent signal emitted by fibronectin on the top of the posts to obtain the deflections of the pillars as a function of time. We used the undeflected pillars (not covered by cells) to determine the resting positions of covered pillars and thus their displacements.

Scanning electron and confocal microscopies

For SEM, we used the procedure previously described by du Roure *et al.*[33] We used a confocal microscope (SP5, Leica, Germany) mounted with a 63× oil immersion objective (Leica, HCX APO 63×/1.4–0.60). We acquired sequentially both Z-stacks and Y-stacks for different fluorophores.

Results

Cell morphology during spreading within the micropillars

To quantitatively study how 3D flexible environments affect cell spreading, we used hexagonal arrays of fibronectin coated micropillars produced by microfabrication techniques (Fig. 1). Only the top of the pillars was coated with fluorescent fibronectin (see methods) to easily track their position through time. The other parts of the substrate were coated with non-fluorescent fibronectin. We used arrays of 5 μm wide and 20 μm high micropillars corresponding to a 23 nN μm^{-1} lateral spring constant. Depending on the pillar density fixed by the pillar to pillar distance (from 4 to 12 μm), REF52 fibroblasts spread within these microstructures (Fig. 1).

We first used fluorescent immunostaining to visualize the cell shapes after they spread into this complex topography. Cells were wrapped around neighboring pillars as shown by the staining of actin cytoskeleton (Fig. 1) and thus presented a different morphology from the one usually observed on continuous 2D substrates. At least ten cells were analyzed for each experiment.

Then we monitored cell spreading at different times from 15 min up to 2 h after their first contact with the substrate. Cells were labeled with calcein to visualize the cell body during spreading and their nucleus labeled with DAPI (Fig. 2). Using confocal microscopy, we found that for a pillar to pillar spacing between 8 and 12 μm, cells usually attached on 3 or 4 adjacent pillars. Cell morphologies varied dramatically with the local environment. Instead of a rounded shape observed for spreading on continuous 2D surfaces,[37,38] the cell periphery exhibited a sequential distribution of inward-curved circular arcs that correlated with the pillar array (Fig. 2). As shown by calcein labelling, the membrane extended around the pillars whereas the cell body and the nucleus were observed in the area in between the pillars (Fig. S1, S2 and Movie S1 and S2‡).

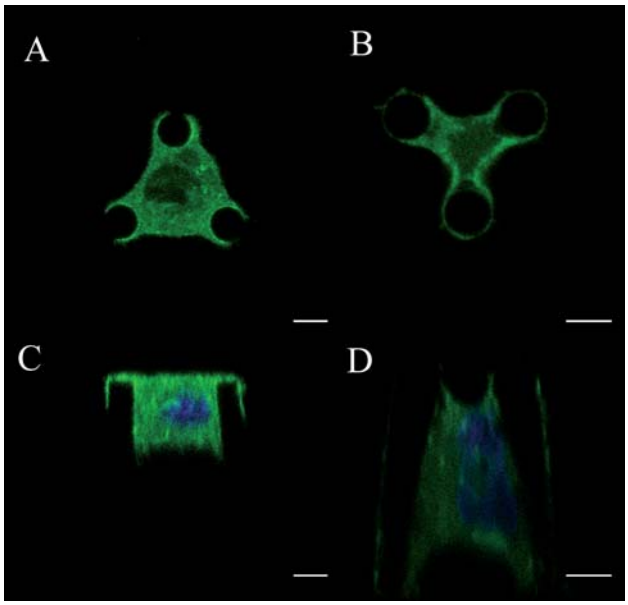

Fig. 2 Spreading of REF52 cells into micropillars. Living cells were first labeled with calcein (green), then fixed for nucleus staining with DAPI (blue). Image stacks were taken with a confocal microscope. (A) Cells were fixed 15 min after their adhesion on the substrate. (B) Cells were fixed 60 min after their adhesion on the substrate. Top views are taken at a height of 5 μm above substrate (A,B) and their corresponding side views are shown below (C,D). Scale bar = 5 μm. Complete confocal stacks are shown in the ESI‡.

As a function of time, cells first attached on top of the pillars, then spread around the pillars whose height was 20 μm to finally establish connections to the flat part of the substrate at $t \approx 1$ h (Fig. 2). Based on confocal microscopy images in the y-z plane acquired at different times from 15 min up to 2 h after plating cells, we obtained the relative position of cells along the pillars and we thus assumed that cell spreading linearly varied with time at a velocity of around 0.3 μm min^{-1} (Fig. 2). For $t < 10$ min, cells were suspended between the pillars without exerting significant deflections on the substrate. Conversely, the pillars were significantly deflected at longer time scales corresponding to an enhanced formation of arc-like cell borders. Such cell morphologies have been previously observed on micropatterned 2D substrates either on substrates made of discrete sites of adhesion[39] or on large adhesive islands with concave shapes.[40] In our study, we observed such arc-like cell morphologies for all the different substrates that we used, including pillar spacings from 4 μm up to 12 μm. Thus we expected that these cell shapes observed during the spreading of fibroblasts within 3D micropatterned substrates could be a robust model for cell invasion in 3D matrices.

Cytoskeleton and focal adhesions organization during cell spreading

To correlate the cell morphologies with intracellular cell tension, we studied the organization of actin cytoskeleton and the distribution and growth of focal adhesions. We imaged REF52

cells, stably transfected with YFP-paxillin used as a reporter, for focal adhesion dynamics. Immunofluorescent staining allowed us to visualize the organization of actin cytoskeleton in response to the micropillar environment (see Materials and methods for details).

In addition to the changes on cellular morphologies during spreading, we observed pronounced modifications in the cytoskeleton and in the adhesion structures. On flat PDMS substrates, one usually observes many prominent stress fibers, unordered and connected to the substrates through focal adhesion structures (Fig. 3). These features were not observed in the case of invasion of a complex 3D substrate. In contrast, we only observed a thick actin stress fiber at the periphery of the cell that surrounded the pillars (Fig. 3).

The arc-like shapes were also evidenced by actin immunostaining, suggesting that the organization of stress fibers dictates the cell shape. These data are in good agreement with previous experiments showing that actin stress fibers could build bridges between adhesive regions.[41,42] However in our case, actin stress fibers do not end up in the vicinity of the micropillars, but they wrap around the microstructures as shown by the continuity of actin staining at the periphery of the cells (Fig. 3B and 3C). Moreover, actin recruitment occurred continuously all along the micropillars for $t > 30$ min. Cell spreading and contractility in 3D micropatterned substrates could thus be driven by the formation of a continuous actin sheet at the cell edge that covered the micropillars.

We monitored the dynamics of focal adhesions since their appearance at the sites where forces are known to be transmitted to the microenvironment on 2D surfaces has been documented.[2] At short time scales ($t < 15$ min), we did not observe the formation of discrete adhesion sites as shown by the recruitment of paxillin using confocal microscopy (Fig. 3C). However, at longer time scales (after 30 min), paxillin proteins were recruited into microstructures that were located not only at the top of the micropillars but also on the surface of the pillars (Fig. 3B). Altogether these data pointed out that cell attachment within 3D environments exhibited a non-standard organization of the actin cytoskeleton, seen as an actin sheet at the periphery of the cell colocalized with the formation of focal adhesions.

Temporal analysis of substrate deformations

To gain new insights into the mechanisms that governed cell contractility in such microenvironments, we used the ability of cells to deform the substrates to quantify the forces they applied (see supplementary movie S3‡). The pillars were sufficiently soft ($k_t = 23$ nN μm^{-1}) to be significantly deflected by the cells. We used micropillars with the same dimensions and we only modified their spacing from 4 up to 12 μm (Fig. 4; Movies S1 & S2‡). To determine the deflections of the pillars as a function of time, their top was labeled with fluorescent fibronectin (Fig. 4) and then the substrate was immersed in non-fluorescent fibronectin. As cells

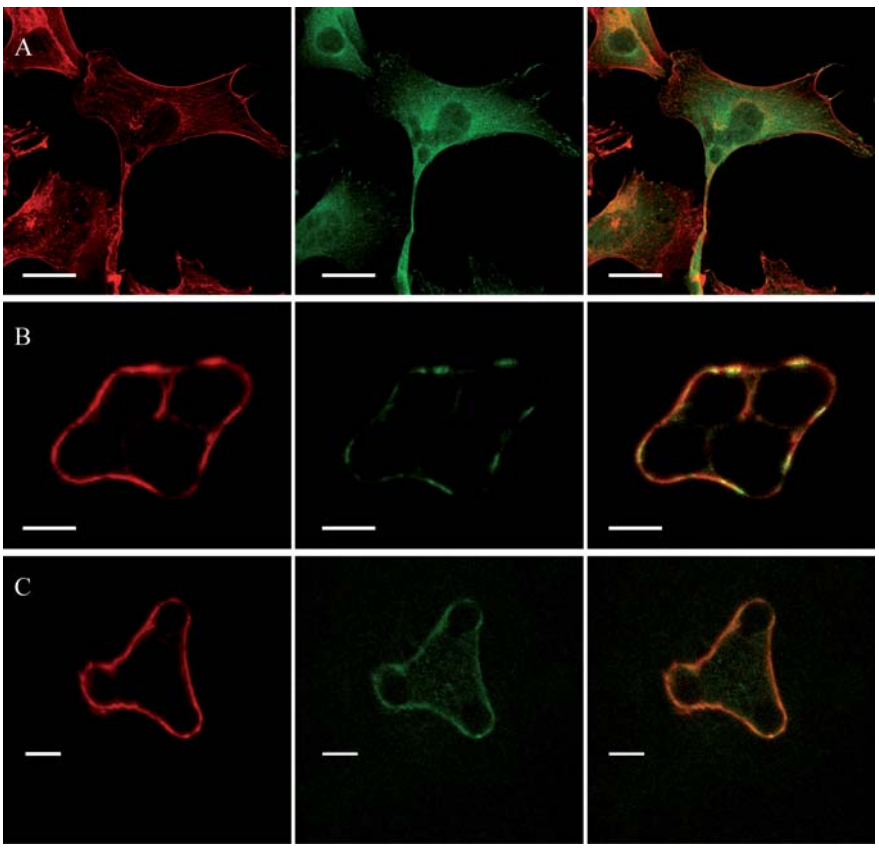

Fig. 3 Confocal images of the immunostaining of the actin cytoskeleton (red) and paxillin (green) on a flat PDMS surface (A, scale bar = 15 μm) and on a micropillar substrate with a 10 μm spacing (B and C, scale bar = 5 μm). Images on the right correspond to the merged image of both channels.

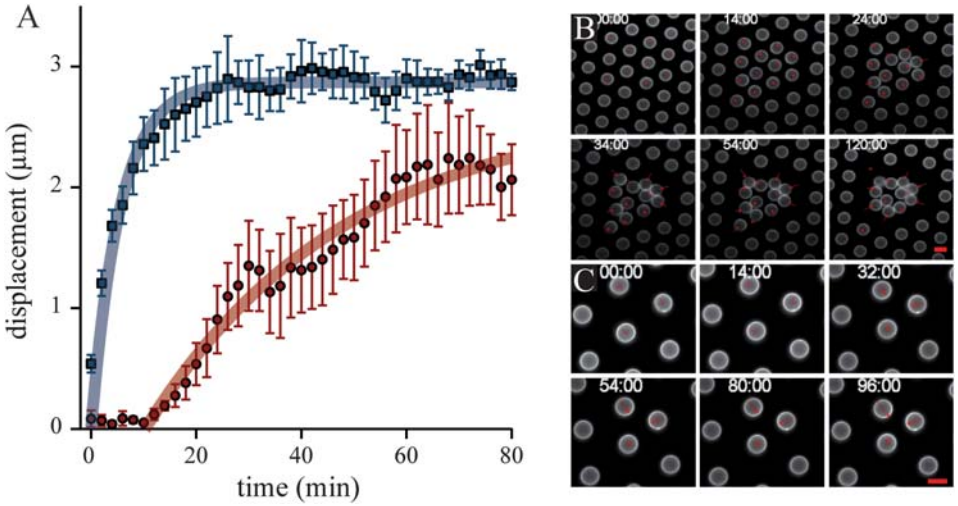

Fig. 4 (A) Displacement of the micropillars as a function of time for two different spacings. The squares correspond to a 4 μm spacing and the circles to a 10 μm spacing (averaged over 10 pillars typically). The curves correspond to an exponential fit, giving an estimate of the displacement rate, *D*. (B) and (C) Sequential epifluorescent images of the displacement of the pillars for 4 μm and 10 μm spacings, respectively. The tops of the pillars were labeled with fluorescent fibronectin. The scale is given by the pillars which are 5 μm in diameter. The arrows represent the displacements of the pillars. The corresponding red scale bar is 2.5 μm. See also Movie S3‡.

expressed YFP-paxillin, we were able to accurately visualize the initial contact of cells with the top of the pillars ($t = 0$).

When cells were plated on pillars with a 4 μm spacing, corresponding to a surface density of 48% (ratio of the surface of pillars over the total surface), we observed a quick increase of the pillar displacement within the first few minutes, up to a saturation *plateau* which was reached after 20 min. The saturation curve was obtained by averaging the displacements of pillars located at the periphery of the cells where the largest deformations were observed. It thus corresponded to a maximal deflection of around 3.2 μm. As shown on the sequential images (Fig. 4), we observed a centripetal movement of the pillars with the largest deformations localized at the cell periphery, similar to what was obtained on 2D surfaces.[11,31,43] However, at long time scales ($t > 30$ min), pillars touched each other. We thus varied the spacing between the pillars to avoid an effect of the geometrical constraints on the substrate deformation. Cells were plated on pillars with a 10 μm spacing (surface density of 16%). On such a substrate, they usually spread over less pillars (3 to 4) than for a 4 μm spacing as shown on Fig. 4. Consequently, we observed different dynamics of the pillar displacement as a function of time. As the initial contact area is smaller on such substrates, the displacement displayed a lag time (~10 min) before observing a significant inward movement of the pillars. The displacement rate, *D*, was also smaller for a 10 μm spacing than for a 4 μm one, 0.1 and 0.4 μm min^{-1} respectively. Altogether our data showed that substrate deformations that we observed when cells dived in between the micropillars were mostly induced by the formation of a thick peripheral actin fiber together with the assembly of focal adhesions along the micropillars.

Beyond 1 h, as cells established contacts with the flat part of the substrate in between the pillars, the cellular contractile machinery could be used not only to deform the pillars by the contraction of actin bundles at the cell periphery but also to pull on the flat part of the substrate. This mechanism could thus partly explain the saturation observed at longer time scales.

Inhibition experiments

To study the role of acto-myosin contractility, we treated REF52 cells with an inhibitor of non-muscle myosin II, blebbistatin.[39,44] Again, we analyzed the displacement of the pillars as a function of time (Fig. 5A). We observed a first step with a quick drop of the pillar displacement followed by a slower relaxation when cells were treated with blebbistatin. Fig. 5A shows an example of the relaxation of the pillars induced by myosin II inhibition of 60%, from 2.8 μm down to 1.2 μm. These results established that the substrate deformations were governed by the contractility of the thick actin bundle observed at the cell edge during the spreading and induced by myosin activity. A reduction of only 60% could be attributed to residual myosin II activities and/or of other myosins. Further experiments should be done to study the influence of myosin inhibition on cell shape within 3D micropatterned substrates.

Influence of the adhesive contact area

To study the influence of the adhesive contact area on cell spreading, we used similar substrates with different coatings. We still used a micro-stamping technique to coat the tip of the pillars with fluorescent fibronectin. We then immersed the substrate with a solution of PEG polymer to prevent cell adhesion in between the pillars.[16,36] Interestingly, we tried both polylysine (PLL)- and maleimide-PEG to backfill the substrates between the pillars. It appeared that cells could adhere in between the pillars, a few micrometres below their top, in the case of PLL-PEG treated substrates, whereas no spreading was observed for maleimide-PEG treatment. We thus used maleimide-PEG to perform the experiments (Fig. 5B).

It appeared that under such conditions, cells adhered only on the top of the substrates without exerting any significant deflection of the pillar when plated over 2 h (Fig. 5B). Cells kept a rounded shape on the substrate. Consequently decreasing the

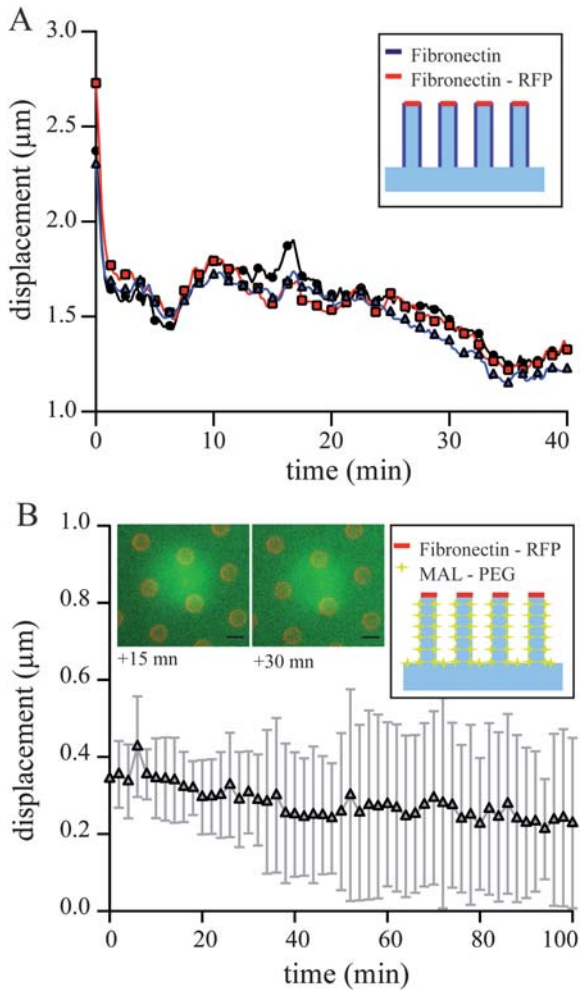

Fig. 5 Influence of myosin II inhibitor and spreading contact area on the deformations of the micropillars. (A) Displacement of three different pillars for blebbistatin treated cells (at $t = 0$) as a function of time. (B) Average displacement of the pillars as a function of time when cells could only adhere on the top of the pillars. Maleimide-PEG (MAL-PEG) was used to prevent cell adhesion in between the pillars.

cell spreading area caused a decrease in actin bundle formation and cytoskeletal tension disabling cells to exert sufficient forces to deform the substrates, as previously observed on 2D surfaces.[31]

Modelling of traction forces exerted by cells within 3D micropatterned substrates

Here we showed that cell contractions were accompanied by displacements of the micropillars localized at the periphery of the cell. We used the theory of elasticity to provide an estimation of the forces acting on the pillars during cell spreading. Our study differed from previous experiments where cells exerted lateral forces on the top of the pillars.[31,33] Here cells spread along the pillars and thus the bending rigidity sensed by the cell varied with the spreading dynamics. Moreover, the distribution of transversal tensions applied by the cell was not known. Based on confocal microscopy observations and inhibition experiments, we assumed that the actin bundle localized around the pillars was the main contributor for force generation. We also observed the formation of an actin sheet following the spreading of the cells along the pillars. So, we hypothesized that forces were continuously distributed along the pillars during cell adhesion.

Considering that the force density (force per unit length) was kept constant along the actin sheet, we used the Euler–Bernouilli beam theory to compute the forces:

$$\frac{d^2x}{dz^2} = -\frac{M(z)}{EI} \quad (1)$$

where z corresponds to the height, $x(z)$ the lateral displacement (see Fig. 1A), E the Young's modulus and I moment of inertia. We assumed that the lower base of the pillars was clamped. Based on our simulations (data not shown), the elasticity of the base led to corrections of less than 10% in the force determination. Hence we used the following conditions: $x(0) = 0$ and $\frac{dx}{dz}(0) = 0$. The torque acting on the pillar was defined as followed:

$$\overrightarrow{M} = \int_{pillar} \overrightarrow{df}(z') \times \overrightarrow{OM} \quad (2)$$

In our model, the force was oriented in the (Ox) axis. Thus we only considered the z component of the vector, $\overrightarrow{OM}$, $z–z'$. We defined the force density as $df(z) = H(z - s)f_0dz$ where $H(z - s)$ is

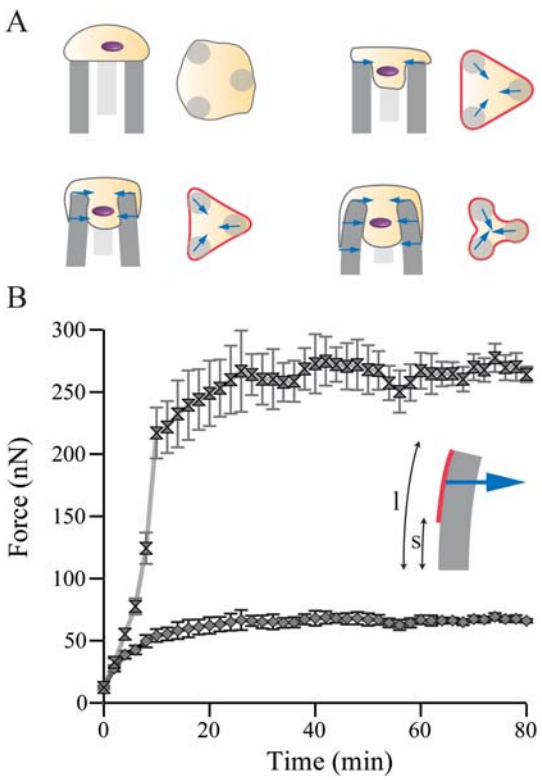

Fig. 6 Calculation of the forces exerted by cells during spreading. (A) Schematic representation of cell spreading and force generation mechanism. (B) Force in nN as a function of time estimated from the assembly of a contractile actin belt around the pillar (upper curve, grey hourglass). As a comparison, we calculated the lateral force exerted only on the top of the pillar according to the measured displacements obtained by video microscopy (lower curve, black diamond).

the Heaviside step function, leading to a null force for $z < s$ (see Fig. 6, insert). The torque was thus given by the following equation:

$$M(z) = \int_0^l H(z'-s)(z-z')f_0 dz' = f_0 \int_s^l (z-z')\, dz'$$

where l is the height of the pillar and s is the remaining area along the pillar, non-covered by cells as shown on Fig. 6B. The force was thus given by: $F = f_0(l-s)$.

Hence, the displacement in the x direction was given by the following equation:

$$x(z) = \frac{F(3(l+s)z^2 - 2z^3}{12\,EI}.$$

By inverting this equation and using $I = \frac{\pi r^4}{4}$ (r is the radius of the pillar), the corresponding force was:

$$F = 3\pi E \frac{r^4}{l^2(l+3s)}\Delta x. \quad (3)$$

According to confocal microscopy images, we assumed that cell spreading was done at a constant velocity, v, of around 0.3 μm min^{-1} up to $s = 0$, $v = \frac{l-s}{t}$. Fig. 6B represents the force as a function of time according to eqn (3). As expected from the displacement of the pillars, our calculation showed that the forces applied by the cell along the pillar quickly increased in the first ten minutes up to a saturation plateau corresponding to forces of around 250 nN. Such forces were in good agreement with previous studies done on heart muscle cells[35] and myoblasts[21] in similar conditions. Based on our model, we arrived at an estimation of forces induced by the contractility of the actin bundle that surrounded the pillars of 250 nN rather than underestimated forces of 60 nN when localized at the top of the pillar (Fig. 6B).

Discussion

While 2D surfaces have been extensively used for cell biology experiments, most cells *in vivo* evolve in a complex 3D environment. Here our approach based on the development of microfabricated substrates with well-defined chemical and mechanical properties served as a useful experimental set-up to probe the ability of cells to adapt their shape to 3D environments. Indeed, cell spreading within 3D micropatterned substrates exhibited different morphologies from the ones observed on 2D surfaces. Here we developed an approach based on the use of microfabricated force sensors combined with epi- and confocal fluorescence microscopies to determine the mechanical forces developed by cells as they spread within 3D microstructures. This method allowed us to measure in real time the deformation and to compute the forces applied by cells. In addition, our force sensors were made in PDMS which allowed different coatings of the substrates to compare the influence of contact spreading area on the generation of forces as well as on the organization of the actin cytoskeleton.

To analyze the influence of substrate topography on cell shape, we studied the adhesion of cells as a function of time within flexible micropillars. It appeared that indeed cells adhered along the pillars and applied forces in the transverse direction. We showed that such forces were generated by the assembly of a contractile actin belt that surrounded the micropillars. The inhibition of non-muscle myosin II with blebbistatin induced a net release of the forces exerted by cells. As shown by actin cytoskeleton staining, the most prominent actin structure appeared at the periphery of the cell and we did not observe the assembly of other stress fibers in the middle of the cell as usually observed on 2D cultures. As cells spread in between the pillars, they formed arc-like shapes that presented an inward curvature that increased with time. In agreement with previous observations on 2D micropatterned substrates,[39] these results confirmed that the cellular contractility increased as cells spread into the pillars. Based on these observations, we thus assumed that the substrate deformations observed in our study were mostly due to this contractile actin network at the cell edge that dictated its shape. We could not exclude that during the spreading of cells within these 3D microenvironments, PDMS micropillar material could be partially taken up through phagocytosis, a cellular function driven by actin polymerization.[45] Further experiments including the localization of specific phagocytocis associated proteins should clarify this point.

During cell spreading, we also observed large deformations of the nucleus as shown in Fig. 2D. The nucleus appeared more deformed with time when large forces were observed. The changes in cell shape induced by the rearrangement of the actin cytoskeleton as well as the increasing contractility could thus be linked to a reorganization of the nucleus, as shown for cell migration within 3D environments.[46] Further experiments should be done to study the precise role of the nucleus and the impact of the microenvironment on nuclear structures. Again, microfabrication substrates would appear to be a useful tool for such experiments since cell migration could be studied in well-defined physical conditions.

Finally, we estimated the forces developed by cells during their spreading. We found a typical value at saturation of 250 nN. However our lack of knowledge about the exact force distribution pattern along the pillar makes this calculation difficult. Since focal adhesions appeared as a major component in the transmission of forces, we checked the distribution of paxillin clusters as well as actin cytoskeleton along the pillars. Both distributions appeared rather as a continuous recruitment than punctuate aggregates (see Supplementary figure S3‡). Hence our calculation was based on the assumption of a constant continuous force density along the pillar. Our results are in good agreement with the global forces exerted by cells as they spread in between deformable surfaces.[21] Even if we consider a discrete distribution of forces along the pillars exerted through adhesion sites, a rough estimate, assuming a force of 5 nN per μm^2 area of focal adhesions,[2,31] leads to a number of around fifty focal adhesions per pillar to generate a 250 nN force. This is compatible with the overall area of the pillar (around 300 μm^2) covered by cells over time. Other components of the focal adhesions could be labeled to confirm this result.

In summary, our approach has enabled the measurement of the mechanical forces exerted by cells within 3D environments. Our findings confirm that cell shape and cytoskeleton organization is strongly affected by the physical and geometrical

properties of the microenvironment. Most of the cells *in vivo* evolve in a 3D matrix with complex physical features such as porosity, topography and elasticity. The use of flexible arrays of micropillars has an important potential as a way to accurately modify these mechanical parameters.

Acknowledgements

The authors thank A. Bershadsky, A. Buguin, N. Biais, M. Coppey, T. Piolot, P. Silberzan, L. Trichet and the group "Biological Physics" from the laboratory MSC for fruitful discussions; A. Richert for cell culture protocols. Confocal microscopy was performed thanks to the Image Facility Center of the Institut Jacques Monod. Financial support from the Association pour la Recherche sur le Cancer (ARC), the C'Nano Ile-de-France, the "Ligue Contre le Cancer" (Comité Ile-de-France), the Association Française contre la Myopathie (AFM), the CNRS "Prise de Risques Interface Physique Biologie", Bonus Qualité Recherche (Université Paris Diderot) and the Agence Nationale de la Recherche (ANR-07-PCVI (Cross-InteCad), ANR-JCh-DiSiP) are gratefully acknowledged. MG acknowledges the ARC for financial support.

References

1 D. A. Lauffenburger and A. F. Horwitz, *Cell*, 1996, **84**, 359–369.
2 N. Q. Balaban, U. S. Schwarz, D. Riveline, P. Goichberg, G. Tzur, I. Sabanay, D. Mahalu, S. Safran, A. Bershadsky, L. Addadi and B. Geiger, *Nat. Cell Biol.*, 2001, **3**, 466–472.
3 B. Geiger and A. Bershadsky, *Curr. Opin. Cell Biol.*, 2001, **13**, 584–592.
4 A. D. Bershadsky, N. Q. Balaban and B. Geiger, *Annu. Rev. Cell Dev. Biol.*, 2003, **19**, 677–695.
5 D. E. Discher, P. Janmey and Y. L. Wang, *Science*, 2005, **310**, 1139–1143.
6 V. Vogel and M. Sheetz, *Nat. Rev. Mol. Cell Biol.*, 2006, **7**, 265–275.
7 O. Chaudhuri, S. H. Parekh, W. A. Lam and D. A. Fletcher, *Nat. Methods*, 2009, **6**, 383–387.
8 A. J. Engler, S. Sen, H. L. Sweeney and D. E. Discher, *Cell*, 2006, **126**, 677–689.
9 D. Riveline, E. Zamir, N. Q. Balaban, U. S. Schwarz, T. Ishizaki, S. Narumiya, Z. Kam, B. Geiger and A. D. Bershadsky, *J. Cell Biol.*, 2001, **153**, 1175–1185.
10 R. J. Pelham and Y. L. Wang, *Proc. Natl. Acad. Sci. U. S. A.*, 1997, **94**, 13661–13665.
11 M. Ghibaudo, A. Saez, L. Trichet, A. Xayaphoummine, J. Browaeys, P. Silberzan, A. Buguin and B. Ladoux, *Soft Matter*, 2008, **4**, 1836–1843.
12 G. Giannone, B. J. Dubin-Thaler, H. G. Dobereiner, N. Kieffer, A. R. Bresnick and M. P. Sheetz, *Cell*, 2004, **116**, 431–443.
13 B. Ladoux, E. Anon, M. Lambert, A. Rabodzey, P. Hersen, A. Buguin, P. Silberzan and R. M. Mege, *Biophys. J.*, 2010, **98**, 534–542.
14 T. Yeung, P. C. Georges, L. A. Flanagan, B. Marg, M. Ortiz, M. Funaki, N. Zahir, W. Y. Ming, V. Weaver and P. A. Janmey, *Cell Motil. Cytoskeleton*, 2005, **60**, 24–34.
15 C. M. Lo, H. B. Wang, M. Dembo and Y. L. Wang, *Biophys. J.*, 2000, **79**, 144–152.
16 A. Saez, M. Ghibaudo, A. Buguin, P. Silberzan and B. Ladoux, *Proc. Natl. Acad. Sci. U. S. A.*, 2007, **104**, 8281–8286.
17 M. Thery, V. Racine, A. Pepin, M. Piel, Y. Chen, J. B. Sibarita and M. Bornens, *Nat. Cell Biol.*, 2005, **7**, 947–953.
18 E. A. Cavalcanti-Adam, T. Volberg, A. Micoulet, H. Kessler, B. Geiger and J. P. Spatz, *Biophys. J.*, 2007, **92**, 2964–2974.
19 P. Friedl and E. B. Brocker, *Cell. Mol. Life Sci.*, 2000, **57**, 41–64.
20 E. Cukierman, R. Pankov and K. M. Yamada, *Curr. Opin. Cell Biol.*, 2002, **14**, 633–639.
21 D. Mitrossilis, J. Fouchard, A. Guiroy, N. Desprat, N. Rodriguez, B. Fabry and A. Asnacios, *Proc. Natl. Acad. Sci. U. S. A.*, 2009, **106**, 18243–18248.
22 C. S. Chen, M. Mrksich, S. Huang, G. M. Whitesides and D. E. Ingber, *Science*, 1997, **276**, 1425–1428.
23 M. Thery, A. Jimenez-Dalmaroni, V. Racine, M. Bornens and F. Julicher, *Nature*, 2007, **447**, 493–U496.
24 A. D. Doyle, F. W. Wang, K. Matsumoto and K. M. Yamada, *J. Cell Biol.*, 2009, **184**, 481–490.
25 T. Steinberg, S. Schulz, J. P. Spatz, N. Grabe, E. Mussig, A. Kohl, G. Komposch and P. Tomakidi, *Nano Lett.*, 2007, **7**, 287–294.
26 A. S. G. Curtis and C. D. Wilkinson, *J. Biomater. Sci., Polym. Ed.*, 1998, **9**, 1313–1329.
27 C. C. Berry, G. Campbell, A. Spadiccino, M. Robertson and A. S. G. Curtis, *Biomaterials*, 2004, **25**, 5781–5788.
28 M. T. Frey, I. Y. Tsai, T. P. Russell, S. K. Hanks and Y. L. Wang, *Biophys. J.*, 2006, **90**, 3774–3782.
29 M. Ghibaudo, L. Trichet, J. Le Digabel, A. Richert, P. Hersen and B. Ladoux, *Biophys. J.*, 2009, **97**, 357–368.
30 Y. Tanaka, K. Morishima, T. Shimizu, A. Kikuchi, M. Yamato, T. Okano and T. Kitamori, *Lab Chip*, 2006, **6**, 230–235.
31 J. L. Tan, J. Tien, D. M. Pirone, D. S. Gray, K. Bhadriraju and C. S. Chen, *Proc. Natl. Acad. Sci. U. S. A.*, 2003, **100**, 1484–1489.
32 X. M. Liang, S. J. Han, J. A. Reems, D. Y. Gao and N. J. Sniadecki, *Lab Chip*, 2010, **10**, 991–998.
33 O. du Roure, A. Saez, A. Buguin, R. H. Austin, P. Chavrier, P. Silberzan and B. Ladoux, *Proc. Natl. Acad. Sci. U. S. A.*, 2005, **102**, 2390–2395.
34 W. R. Legant, A. Pathak, M. T. Yang, V. S. Deshpande, R. M. McMeeking and C. S. Chen, *Proc. Natl. Acad. Sci. U. S. A.*, 2009, **106**, 10097–10102.
35 A. Kajzar, C. M. Cesa, N. Kirchgessner, B. Hoffman and R. Merkel, *Biophys. J.*, 2008, **94**, 1854–1866.
36 J. Fink, M. Thery, A. Azioune, R. Dupont, F. Chatelain, M. Bornens and M. Piel, *Lab Chip*, 2007, **7**, 672–680.
37 B. J. Dubin-Thaler, G. Giannone, H. G. Dobereiner and M. P. Sheetz, *Biophys. J.*, 2004, **86**, 1794–1806.
38 D. Cuvelier, M. Thery, Y. S. Chu, S. Dufour, J. P. Thiery, M. Bornens, P. Nassoy and L. Mahadevan, *Curr. Biol.*, 2007, **17**, 694–699.
39 I. B. Bischofs, F. Klein, D. Lehnert, M. Bastmeyer and U. S. Schwarz, *Biophys. J.*, 2008, **95**, 3488–3496.
40 M. Thery, V. Racine, M. Piel, A. Pepin, A. Dimitrov, Y. Chen, J. B. Sibarita and M. Bornens, *Proc. Natl. Acad. Sci. U. S. A.*, 2006, **103**, 19771–19776.
41 M. Thery, A. Pepin, E. Dressaire, Y. Chen and M. Bornens, *Cell Motil. Cytoskeleton*, 2006, **63**, 341–355.
42 O. M. Rossier, N. Gauthier, N. Biais, W. Vonnegut, M. A. Fardin, P. Avigan, E. R. Heller, A. Mathur, S. Ghassemi, M. S. Koeckert, J. C. Hone and M. P. Sheetz, *EMBO J.*, 2010, **29**, 1055–1068.
43 S. Munevar, Y. L. Wang and M. Dembo, *Biophys. J.*, 2001, **80**, 1744–1757.
44 Y. F. Cai, O. Rossier, N. C. Gauthier, N. Biais, M. A. Fardin, X. Zhang, L. W. Miller, B. Ladoux, V. W. Cornish and M. P. Sheetz, *J. Cell Sci.*, 2010, **123**, 413–423.
45 F. Castellano, P. Chavrier and E. Caron, *Semin. Immunol.*, 2001, **13**, 347–355.
46 K. Wolf and P. Friedl, *Clin. Exp. Metastasis*, 2009, **26**, 289–298.

